Received: 21 February 2024 | Revised: 7 May 2024 | Accepted: 13 May 2024

DOI: 10.1002/ese3.1798

ORIGINAL ARTICLE

Optimal scheduling of regional integrated energy systems with hot dry rock enhanced geothermal system based on information gap decision theory

Qingfeng Liu[1] | **Mohamed A. Mohamed**[2] | **Adrian Ilinca**[3] | **Andres Annuk**[4] | **Emad Abouel Nasr**[5]

[1]College of Electrical and New Energy, China Three Gorges University, Yichang, China

[2]Electrical Engineering Department, Faculty of Engineering, Minia University, Minia, Egypt

[3]Department of Mechanical Engineering, École de Technologie Supérieure, Montréal, Québec, Canada

[4]Institute of Forestry and Engineering, Estonian University of Life Sciences, Tartu, Estonia

[5]Department of Industrial Engineering, College of Engineering, King Saud University, Riyadh, Saudi Arabia

Correspondence
Mohamed A. Mohamed, Electrical Engineering Department, Faculty of Engineering, Minia University, Minia 61519, Egypt.
Email: dr.mohamed.abdelaziz@mu.edu.eg

Adrian Ilinca, Department of Mechanical Engineering, École de Technologie Supérieure, Montréal, QC H3C 1K3, Canada.
Email: adrian.ilinca@etsmtl.ca

Funding information
King Saud University,
Grant/Award Number: Researchers Supporting Project number RSP2024R164

Abstract

Hot dry rock (HDR) is regarded as a promising resource of geothermal energy and becomes an important field for future geothermal development due to its advantages of high temperature, wide distribution and huge reserves. At present, HDR research is mainly focused on the modeling and efficiency evaluation of power generation cycle, but its relationship with the source side of the system has not been considered in the field of integrated energy systems. Therefore, this paper proposes a day-ahead scheduling method for regional integrated energy systems (RIES) with HDR based on information gap decision theory (IGDT). First, the heat transfer system model of HDR is established according to the energy flow model and basic structure of the HDR enhanced geothermal system (EGS). Second, a comprehensive geothermal energy system scheduling model is established from HDR based on the energy hub modeling structure. Then, the IGDT is introduced to analyze the renewable energy output uncertainty in the model. Finally, through a real RIES analysis, the simulation results verified the correctness and effectiveness of the proposed model. The scheduling cost was ¥47,073 when EGS participated in the scheduling. Access to EGS reduced the system's total 24-h energy purchase by 8305 kW, natural gas consumption by 3051.9 m^3, and total carbon emissions by 742.28 kg. The latter emphasized that the proposed model achieves the purpose of reducing the system cost, saving energy and reducing emissions.

KEYWORDS
day-ahead scheduling, dry hot rock enhanced geothermal system, energy hub, information decision theory, regional integrated energy systems

1 | INTRODUCTION

Nowadays, many countries in the world are conducting research on new energy, especially renewable energy, to reduce their dependence on traditional fossil fuels.[1] Geothermal energy compared to other renewable energy sources has the advantages of abundant energy storage, stable production, and no chemical pollution. However, due to the limitations of drilling, fracturing, flow heating, and other technologies, the development of geothermal power generation is not obvious.[2] The enhanced development of geothermal systems will accelerate the extraction and utilization of geothermal energy.[3] Hot dry rock (HDR) is a new type of geothermal energy that can be exploited in the belt, which is generally stored in low-porosity and low-permeability rocks within 3–10 km underground at temperatures between 150°C and 650°C.[4] It is estimated that the total amount of HDR resources in mainland China is 2.52×1025 J, equivalent to 860×1012 t of standard coal. If calculated according to 2% of recoverable resources, it is equivalent to 5300 times the current total annual energy consumption in China.[5] Hence, the development and utilization of HDR play a crucial role in China's early realization of carbon peak and neutrality.[6] The enhanced geothermal system (EGS) extracts and utilizes geothermal resources by creating artificial fractures in HDR.[7] At present, the research on HDR development focuses on the thermal storage mining process and efficiency evaluation. For example, Al-Kbodi et al.[8] introduces a comprehensive comparative numerical investigation of innovative U-tube ground heat exchangers with a hollow-finned structure for augmenting the performance of the ground couple heat pumps (GCHPs). Al-Kbodi et al.[9] explains the development of traditional circular 2U-tube borehole heat exchangers (BHEs) that makes an optimally designed model for maximizing the heat extraction rates and minimizing the energy consumption characteristics and BHE number. Zayed et al.[10] introduces numerical simulation methods for geothermal systems as a framework for the scale and design of geothermal power plants. Rajeh et al.[11] introduces a detailed comparative numerical study on a novel coaxial ground heat exchanger with an oval cross-section for enhancing the performance of the GCHP.

Another issue is the strong uncertainty in the renewable energy system within the regional integrated energy systems (RIES). To deal with the uncertainty, the two-point estimation method was used to describe the uncertainty in wind speed, light intensity and load.[12] This method is simple, but the modeling accuracy is relatively poor, and it is difficult to directly guide the production practice. Tan et al.[13] predicts wind power output based on the scenario method. Although uncertainty can be accurately described, its computation cost is high and it is difficult to obtain the distribution of uncertainty parameters. Tu et al.[14] proposes an economic scheduling model based on opportunity-constrained programming. The stochastic optimization method is somewhat subjective. There is a close correlation between the optimal solution set and the probability distribution of uncertain parameters. In the study Zhang et al.,[15] the authors proposed a robust two-stage distributed optimal scheduling model, which sacrifices the system economy to ensure its robustness. As a method to study the variation range of uncertain parameters, the information gap decision theory (IGDT) requires less information and has high computational efficiency. It provides the decision-making basis from both robust and economic aspects. The effect of gap value on target disturbance is also analyzed and satisfies the need of controlling uncertain parameters in actual industrial process.

To sum up, in the field of integrated energy systems, the link between HDR and the source side of the system has not been considered. Therefore, this paper proposes a day-ahead scheduling method of integrated energy systems in geothermal areas containing HDR based on IGDT. The main contributions of this paper are as follows.

1. According to the working principle and basic structure of EGS, the operating model of EGS is constructed. A fully renewable system model based on HDR-wind-solar hub is established through the energy hub to establish the connection between input and output. The influence of EGS participating in RIES scheduling is studied.
2. Considering the uncertainty in wind and photovoltaic power, an optimal scheduling model of RIES is constructed based on IGDT. The uncertainty in the system is handled from two aspects to avoid risks and seek opportunities, and a bidirectional scheduling strategy is provided for decision-makers.

The rest of the paper is arranged as follows. Section 2 introduces the basic structure and operation model of EGS. Section 3 presents the scheduling model. In Section 4, the stochastic scheduling model based on IGDT is discussed. In Section 5, the effectiveness of the proposed method is demonstrated. Section 6 presents the conclusion and the future research.

2 | THE BASIC STRUCTURE AND OPERATION MODEL OF EGS

The HDR geothermal power plant includes an underground part and an above-ground part as shown in Figure 1. The underground part consists of injection wells, production wells and fractured thermal reservoirs. The above-ground part is composed of a reservoir, water pumping station, and a generator set. The injection well injects a low-temperature fluid into the fractured reservoir for heat exchange with the high-temperature rock mass. The heated fluid is returned to the surface through the production wells to generate electricity. These fluids then exchange energy in evaporators and heat exchangers. The heat generated provides thermal and electrical output to the system through a shunt. Finally, the cooled fluid is recirculated through the injection well for the next time. HDR geothermal power plants convert geothermal energy into electricity and heat through EGS, and the extracted energy can be used for integrated energy system optimization scheduling.

2.1 | Basic structure of EGS in HDR

At present, there are three main power generation systems for geothermal power plants. Flash evaporation electric system, Kalina cycle system and organic Rankine cycle (ORC) system. The structure of the flash evaporation electric system is simple, but the equipment is large and the efficiency is low. The efficiency of the Karina cycle is high, but the equipment stris complex and the circulation pressure is high. The ORC is relatively widely used due to its high efficiency and simple structure.[12]

The EGS includes evaporators, turbine-generators, condensers and working medium pumps as shown in Figure 2. During EGS operation, the organic working fluid in the evaporator is heated by the production well fluid and partially vaporized at certain dryness. The separated high-temperature saturated steam drives a turbine generator to do work and generate electricity. Turbine exhaust gas enters the condenser and is converted into a saturated liquid by heat exchange with cooling water. Then it is pressurized by the working pump into the heat exchanger, and the saturated liquid in the evaporator is mixed with the organic working medium of the heat exchanger. In the heat exchanger it is heated by high-temperature fluid from the evaporator. Finally, the organic working fluid is sent to the evaporator for circulation, and the fluid from the heat exchanger enters the water injection well for circulation.

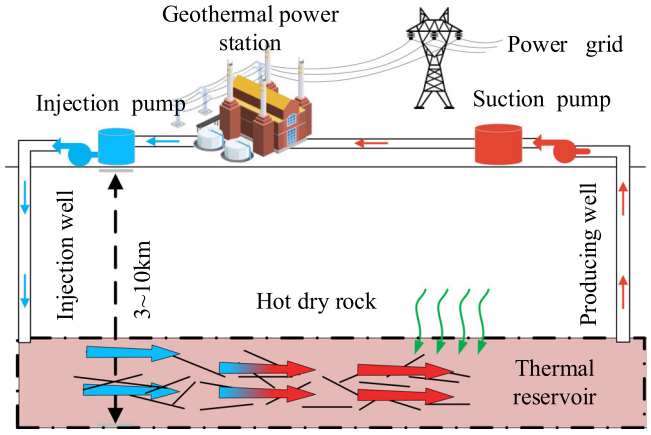

FIGURE 1 Operation of HDR geothermal power plant.

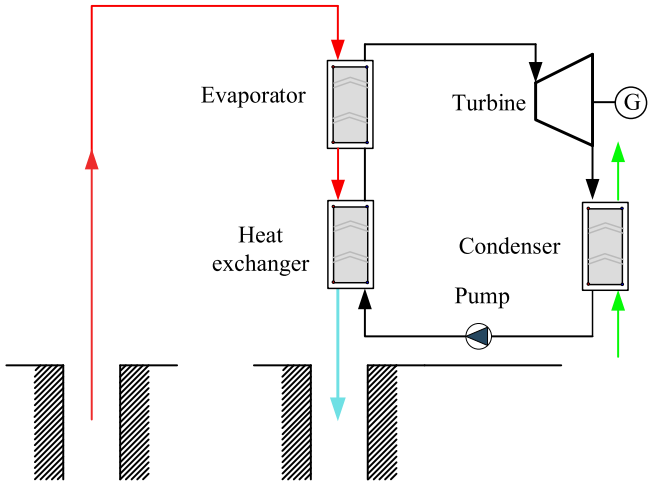

FIGURE 2 EGS structure diagram.

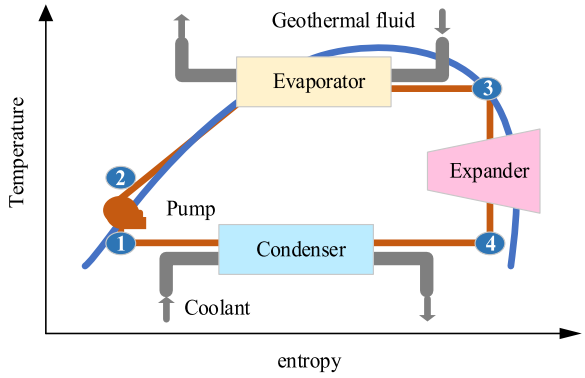

FIGURE 3 Thermodynamic process diagram of ORC system.

2.2 | EGS operation model

Figure 3 shows the thermodynamic process diagram of the ORC working medium. Medium entropy pressure of working pump in (1-2), constant pressure heat

absorption of the evaporator (2-3), isentropic expansion of expansion machine (3-4), and constant pressure cooling of the condenser (4-1).[16,17]

The heat production power H_t^{geo} of EGS at time t can be expressed as follows:

$$H_t^{geo} = m_t^{geo} c_p \left(T_w^{pro} - T_w^{inj} \right), \tag{1}$$

where m_t^{geo} is the mass flow rate of the hot water production well at time t. c_p is the specific heat capacity of geothermal fluid. T_w^{inj} and T_w^{pro} are the injection temperature and outlet temperature of geothermal fluid, respectively.

Due to the limitations of production well pipe size and output power of the water pumping station, as well as mineral factors in the rock mass, the mass flow rate of hot water extraction at time t needs to meet the following constraints[16]:

$$u_t m^{geo,min} \le m_t^{geo} \le u_t m^{geo,max}, \tag{2}$$

where $m^{geo,\max}$ and $m^{geo,\min}$ are the upper limit and lower limit of fluid flow, respectively. u_t is the 0-1 variable of the operating state of the geothermal generator set.

The heat energy extracted from the HDR is distributed flexibly between the power generation system and the heating system by diverting valves. The heat distribution model is expressed as follows:

$$\begin{cases} m_t^h = m_t^{geo} \times \alpha_t, 0 \le \alpha_t \le 1 \\ m_t^e = m_t^{geo} \times \beta_t, 0 \le \beta_t \le 1 \\ \alpha_t + \beta_t = 1 \end{cases}, \tag{3}$$

where m_t^h is the fluid flow for heating at time t, and m_t^e is the fluid flow for power generation at time t. α_t and β_t are the ratio factor for the allocation of geothermal energy to the heating system and power supply system at time t.

The energy balance model in the diverter valve is described as follows:

$$\begin{cases} m_t^{geo} T_w^{pro} = m_t^e T_e^{inj} + m_t^q T_q^{inj} \\ H_t^h = m_t^h c_p (T_h^{pro} - T_h^{inj}) \\ H_t^e = m_t^e c_p (T_e^{pro} - T_e^{inj}) \end{cases}, \tag{4}$$

where H_t^h is the thermal power used for heating at time t. H_t^e is the thermal power used for power generation at time t. T_h^{pro} and T_h^{inj} are the fluid temperatures at the inlet and outlet of the heating system, respectively. T_e^{pro} and T_e^{inj} are fluid temperatures at the outlet and inlet of the power generation system, respectively.

The working fluid flow rate of the working pump at time t is m_t^{pump}. The temperature of the outlet and inlet fluid of the working pump is T_p^{inj} and T_p^{pro}, and the working efficiency of the pump is η_p. The power consumption of the pump at time t can be expressed as[18]:

$$P_t^{pump} = m_t^{pump} c_p (T_p^{pro} - T_p^{inj}) / \eta_p, \tag{5}$$

The thermal conversion efficiency of ORC is defined as the ratio of output power to absorbed heat power, and its value changes with the change of the input thermal power within a certain range. Let the average conversion efficiency of ORC be η^{geo}. The output electrical power P_t^{EGS} of EGS at time t can be expressed as follows:

$$P_t^{EGS} = \eta^{geo} H_t^e - P_t^{pump}. \tag{6}$$

In the process of heat transmission, if the heat loss is η^{loss}, the output thermal power of EGS at time t can be expressed as follow:

$$H_t^{EGS} = (1 - \eta^{loss}) H_t^h. \tag{7}$$

During the operation of the dry hot rock geothermal power station, the temperature of the dry hot rock around the geothermal reservoir will decrease year by year as the heat energy is continuously extracted.

The operation and maintenance cost of HDR geothermal power station mainly includes the cost of material consumption and the cost of electric pump consumption. The operating cost of EGS during the t period can be expressed as follow[19,20]:

$$f_t^{EGS} = \sum_t^{24} m_t^{geo} \times p_w + \sum_t^{24} \left(P_t^{pump} \times p_t^{price} \right), \tag{8}$$

where p_w is the unit price of the fluid medium and p_t^{price} is the unit price of electricity purchased at time t.

3 | SCHEDULING MODEL

To uniformly model the equipment in the RIES, the system is regarded as a two-port network as shown in Figure 4. Based on the energy hub model, the conversion relationship between various energy inputs and outputs is established.

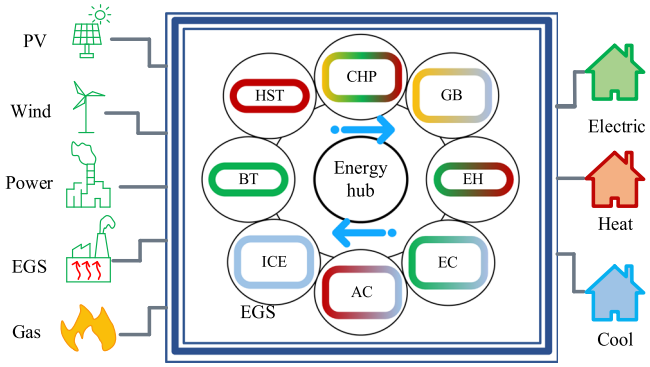

FIGURE 4 Regional energy hub architecture with EGS.

3.1 | Energy hub model

The architecture mainly includes energy input, energy conversion, energy transport, energy storage and energy balance. Each part is modeled as follows:

3.1.1 | Transformation model of energy device

1. Cogeneration units.

$$Q_{t,gas}^{chp}\eta_{chp,e} = P_t^{chp}, \tag{9}$$

$$Q_{t,gas}^{chp}\eta_{chp,h} = H_t^{chp}, \tag{10}$$

where $Q_{t,gas}^{chp}$ is the quantity of natural gas being supplied to the cogeneration unit at time t. $\eta_{chp,e}$ and $\eta_{chp,h}$ are the cogeneration unit's efficiency in converting gas to electricity and heat, respectively.

2. Gas-fired boilers.

$$Q_{t,gas}^{gb}\eta_{gb} = H_t^{gb}, \tag{11}$$

$$P_{gb}^{\min} \le P_{gb} \le P_{gb}^{\max}, \tag{12}$$

where $Q_{t,gas}^{gb}$ is the quantity of natural gas being supplied to the gas boiler at time t. η_{gb} is the gas-heat conversion efficiency of the gas-fired boiler. H_t^{gb} is the output thermal power at time t.

3. Electric refrigerator.

$$P_t^{ec}\eta_{ec} = C_t^{ec}, \tag{13}$$

$$P_{ec}^{\min} \le P_{ec} \le P_{ec}^{\max}, \tag{14}$$

where P_t^{ec} is the electric power consumed by the electric refrigerator at time t. η_{ec} is the electric-thermal conversion efficiency of an electric heat pump.

4. Absorption refrigerator.

$$H_t^{ac}\eta_{ac} = C_t^{ac}, \tag{15}$$

$$P_{ec}^{\min} \le P_{ec} \le P_{ec}^{\max}, \tag{16}$$

where H_t^{ac} is the thermal power consumed by the absorption refrigerator at time t. η_{ac} is the heat-cold conversion efficiency of the absorption refrigerator.

5. Ice storage air conditioning.

$$P_t^{ice}\eta_{ice} = C_t^{in}, \tag{17}$$

where P_t^{ice} is the electric power consumed by ice storage air conditioning at time t. η_{ice} is the refrigeration coefficient of ice storage air conditioning. C_t^{in} is the ice-making power of the ice storage air conditioner at time t.

3.1.2 | Energy storage device model

The generalized energy storage device can store the excess energy at a certain time and release it at other times of demand, which is a two-way conversion process of energy conversion.

$$Q_{x,t} - Q_{x,t-1} = X_{t-1}^{in}\eta_x^{in} - X_{t-1}^{out}/\eta_x^{out}, \tag{18}$$

$$0 \le X_t^{in} \le X_{\max}^{in}, \tag{19}$$

$$0 \le X_t^{out} \le X_{\max}^{out}, \tag{20}$$

$$Q_{x,24} = Q_{x,1}, \tag{21}$$

$$Q_x^{\min} \le Q_{x,t} \le Q_x^{\max}. \tag{22}$$

In formulas (20) and (21), X represents the type of energy. Electricity, heat and cold are respectively represented by P, H, and C. $Q_{x,t}$ and $Q_{x,t-1}$ are the storage capacity of the energy storage system at time t and $t-1$, respectively. X_t^{out} and X_t^{in} are the output and input rated power of the energy storage system at time t, respectively. η_x^{out} and η_x^{in} are the output and input efficiencies of the energy storage system, respectively.

3.1.3 | Energy flow model

The energy flow model of the energy network is described by the energy hub model. The balance between the power grid, heat network and cold network is simplified as follows:

1. Electric power balance.

$$P_t^{EGS} + P_t^{w} + P_t^{pv} + P_t^{chp} + P_t^{grid} + P_t^{out} - P_t^{ec} - P_t^{ice} - P_t^{in} = P_t^{load} \tag{23}$$

where, P_t^{w} is the generation power of wind energy at time t. P_t^{pv} is the power generation of photovoltaic at time t. P_t^{grid} is the electrical power purchased by the area system at time t. P_t^{load} is the electrical load of the system at time t.

2. Thermal power balance.

$$H_t^{EGS} + H_t^{chp} + H_t^{gb} + H_t^{out} - H_t^{ac} - H_t^{in} = H_t^{load}, \tag{24}$$

where H_t^{load} is the heat load of the system at time t.

3. Cold power balance.

$$C_t^{ec} + C_t^{ac} + C_t^{out} = C_t^{load}, \tag{25}$$

where C_t^{load} is the cooling load of the system at time t.

3.2 | Objective function

The optimization objective of the RIES is the daily operating cost. Including electricity purchase cost f^{grid}, gas purchase cost f^{gas}, EGS cost f^{EGS}, and carbon emission cost f^{ce}. The objective function can be expressed as follows:

$$\min F = \sum_{t=1}^{24} \left(f_t^{grid} + f_t^{gas} + f_t^{EGS} + f_t^{ce} \right), \tag{26}$$

$$f_t^{grid} = P_t^{grid} p_{price}, \tag{27}$$

$$f_t^{gas} = Q_{gas} p_{gas}, \tag{28}$$

$$f_t^{ce} = \varepsilon \left(\beta_e P_t^{grid} + \beta_g Q_t^{gas} \right), \tag{29}$$

where p_t^{price} is the unit price of electricity purchase at time t (¥/kWh). p_t^{gas} is the unit price of the gas purchased at time t (¥/m^3). ε is the carbon emission unit price (¥/kg). β_e and β_g are equivalent emission coefficients of electricity purchase and gas purchase, respectively.

3.3 | Constraints

3.3.1 | Energy input constraint

1. Power purchase constraints.

$$P_{grid}^{\min} \le P_t^{grid} \le P_{grid}^{\max}, \tag{30}$$

where, $P_{grid}^{\min}$ and $P_{grid}^{\max}$ indicate the maximum and minimum values of power purchase, respectively.

2. Natural gas constraints.

$$Q_{t,gas} = Q_{t,gas}^{chp} + Q_{t,gas}^{gb}, \tag{31}$$

$$Q_{gas}^{\min} \le Q_{t,gas} \le Q_{gas}^{max}, \tag{32}$$

where $Q_{t,gas}$ is the amount of natural gas purchased by the regional system at time t. $Q_{gas}^{\min}$ and $Q_{gas}^{\max}$ are the maximum and minimum volumes purchased, respectively.

3. Photovoltaic power generation constraints.

$$0 \le P_t^{pv} \le P_{pv}^{\max}, \tag{33}$$

where $P_{pv}^{\min}$ and $P_{pv}^{\max}$ are the maximum and minimum value of photovoltaic output, respectively.

4. Wind power generation constraints.

$$P_w^{\min} \le P_t^{w} \le P_w^{\max}, \tag{34}$$

where $P_w^{\min}$ and $P_w^{\max}$ are the maximum and minimum values of wind power generation, respectively.

5. EGS constraints.

$$P_{\min}^{EGS} \le P_t^{EGS} \le P_{\max}^{EGS}, \tag{35}$$

$$H_{\min}^{EGS} \le H_t^{EGS} \le H_{\max}^{EGS}, \tag{36}$$

where $P_{\min}^{EGS}$ and $P_{\max}^{EGS}$ are the minimum and maximum power supply for EGS, respectively. $H_{\min}^{EGS}$ and $H_{\max}^{EGS}$ are the minimum and maximum values of EGS heating power, respectively.

3.3.2 | Energy conversion constraints

The constraints of energy conversion between EGS, gas turbines, gas boilers, electric chillers, absorption chillers and ice storage air conditioners should meet Equations (1)–(17).

3.3.3 | Energy storage constraint

Storage battery, heat storage irrigation and ice storage system, energy storage constraints should meet Equations (18)–(22).

3.3.4 | Energy flow constraint

In the RIES, the energy hub plays the role of connecting the conversion between different energies. It requires the input and output energy to maintain a dynamic balance, and its energy flow constraints should meet Equations (23)–(25).

4 | STOCHASTIC SCHEDULING MODEL BASED ON IGDT

4.1 | IGDT model

IGDT consists of system model, operation requirement and uncertainty set model. The system model for the cost optimization problem is expressed as follows:

$$\begin{cases} \min & f(s,w) \\ s.\ t & H(s,w)=0 \\ & \mathrm{G(s,w)} \geq 0 \end{cases} \tag{37}$$

where s and w are decision variables and uncertain parameters. H and G are bound bundles of equality and inequality.

In this paper, the envelope constraint model of IGDT is used to represent the uncertainty parameter $\widetilde{w}$, which is expressed as follows:

$$U(\alpha,\widetilde{w})=\left\{w:\left|\frac{w-\widetilde{w}}{\widetilde{w}}\right|\leq\alpha\right\}, \tag{38}$$

where α is the uncertainty, which represents the information gap between a known predicted value and an unknown actual value. $U(\alpha,\widetilde{w})$ indicates that the uncertainty parameters does not deviate from the predicted value by more than α.

In the uncertain parameter environment, the robust model represents the system's resistance to the change of the maximum uncertain parameter. The opportunity model represents the return on the change of the minimum uncertainty parameter. The corresponding mathematical models of the two strategies are expressed as follows:

$$\begin{cases} \max \alpha_r & \\ s.\ t. & \max\limits_{X} f(s,w)\leq f_r \\ & f_r=(1+\theta_r)f_0 \\ & \forall\ w\in U(\alpha_r,\widetilde{w}) \\ & H(s,w)=0 \\ & G(s,w)\geq 0 \end{cases} \tag{39}$$

$$\begin{cases} \min \alpha_o & \\ s.\ t. & \min\limits_{X} f(s,w)\leq f_o \\ & f_o=(1-\theta_o)f_0 \\ & \exists\ w\in U(\alpha_o,\widetilde{w}) \\ & H(s,w)=0 \\ & G(s,w)\geq 0 \end{cases} \tag{40}$$

where α_r and α_o are the variable ranges of the uncertain parameters in the robust strategy or chance strategy. f_0 is to determine the objective function value under the model. θ_r, θ_o are robust factors and opportunity factors, indicating the degree of deviation that scheduling costs are higher or lower than f_0. $\max f$ and $\min f$ are the maximum and minimum functions of the uncertainty parameter w, respectively.

Equations (39) and (40) are the two-layer optimization model. The upper layer solution satisfies the maximum uncertainty of the preset target. The lower layer solves the maximum operating cost of the system under uncertainty fluctuation. In the lower model, the lower the output of associated resources, the more external energy purchase by the system. The higher the load demand, the greater the system energy consumption. Therefore, for a given uncertainty range, the maximum operating cost of the lower model occurs where the associated resource production is lowest and the load demand is highest. At this time, the two-layer optimization model of Equations (39) and (40) can be equally transformed into a single-layer optimization model, as shown in Equations (41) and (42)[22–24]:

$$\begin{cases} \max \alpha_r \\ s.\ t. \quad f(s,w) \le f_c \\ \quad\quad f_c = (1+\beta_c) f_0 \\ \quad\quad \mathrm{w} = (1-\alpha)\widetilde{w} \\ \quad\quad H(s,w) = 0 \\ \quad\quad G(s,w) \ge 0 \end{cases} \tag{41}$$

$$\begin{cases} \min \alpha_o \\ s.\ t. \quad f(s,w) \le f_o \\ \quad\quad f_o = (1-\beta_w) f_0 \\ \quad\quad \mathrm{w} = (1+\alpha)\widetilde{w} \\ \quad\quad H(s,w) = 0 \\ \quad\quad G(s,w) \ge 0 \end{cases} \tag{42}$$

4.2 | IGDT steps

The steps of the IGDT are described as shown in Figure 5:

1. Input the basic data of the RIES deterministic model.
2. With the goal of minimizing the daily operating cost, the objective function f_0 is obtained by simulating the deterministic model.
3. Decision-makers set the subjective bias factor of the robust model and chance model θ_r, θ_o. Adding uncertain system models separately. The prediction error α and corresponding scheduling strategy are obtained.
4. Calculate the variation amplitude of uncertain parameters α_r, α_o and scheduling cost f under different strategies. Make the corresponding unit output plan and scheduling plan.[21]

5 | EXAMPLE ANALYSIS

The integrated energy system scheduling model of the geothermal area containing HDR is a mixed integer linear programming model, which can be solved by CPLEX solver based on YALMIP. This paper takes the HDR resource-rich area of Gonghe Basin in Qinghai Province, China as the research object.[25] A typical autumn day in this area is taken as an example of optimizing scheduling.

The time of use price adopted in this paper is shown in Table 1. Parameters of various energy storage devices in this paper are shown in Table 2. Equipment parameters are shown in Table 3. EGS parameters are shown in Table 4. The cost price parameters are shown in Table 5. The 24 h wind power, light power and load demand forecast curves are shown in Figure 6. Assume the load power,

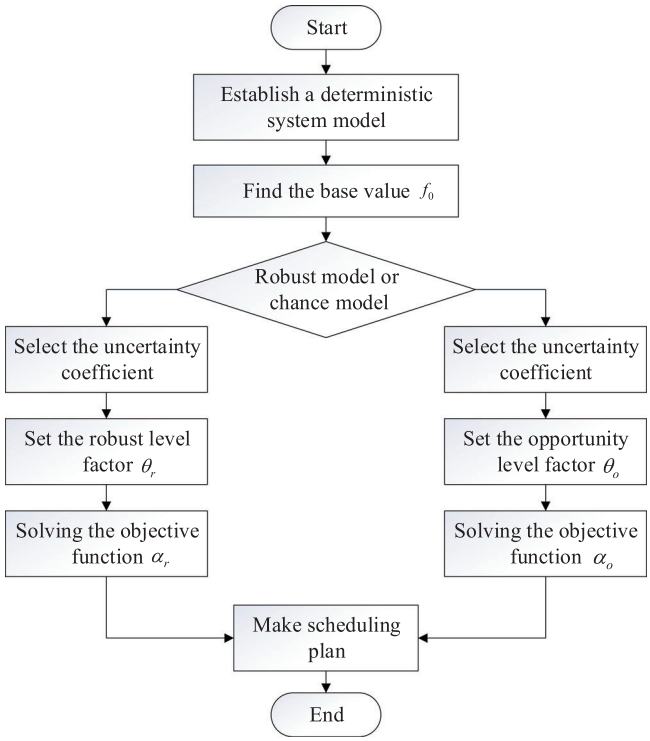

FIGURE 5 IGDT flowchart.

TABLE 1 TOU electricity price.

Time	Purchase price
1–7, 23–24	0.48
8–11, 15–18	0.88
12–14, 19–22	1.10

TABLE 2 Parameters of energy storage equipment.

$P_{es,c}^{\max}$	$P_{es,d}^{\max}$	$E_{es}^{\min}$	$E_{es}^{\max}$	$\eta_{es,c}$	$\eta_{es,d}$
500 kW	700 kW	400 kW h	1800 kW h	0.96	0.96
$P_{hs,c}^{\max}$	$P_{hs,d}^{\max}$	$E_{hs}^{\min}$	$E_{hs}^{\max}$	$\eta_{hs,c}$	$\eta_{hs,d}$
800 kW	800kW	400 kW·h	1800kW·h	0.98	0.98
$P_{cs,c}^{\max}$	$P_{cs,d}^{\max}$	$E_{cs}^{\min}$	$E_{cs}^{\max}$	$\eta_{cs,c}$	$\eta_{cs,d}$
700 kW	800 kW	400 kW h	1800kw h	0.97	0.95

TABLE 3 Parameters of energy conversion equipment.

$P_{\mathrm{chp}}^{\max}$	$H_{\mathrm{gb}}^{\max}$	$H_{\mathrm{ac}}^{\max}$	$P_{ec}^{\max}$	$P_{\mathrm{ice}}^{\max}$	$P_{\mathrm{pv}}^{\max}$
2000 kW	1300 kW	1000 kW	500 kW	200 kW	600 kW
$P_{w}^{\max}$	$\eta_{\mathrm{chp},e}$	$\eta_{chp,h}$	η_t	C_{ec}	C_{ice}
700 kW	0.3	0.45	0.98	4	3.5

equipment parameters and price parameters remain unchanged in the simulation time step, and there is no error in data prediction.

5.1 | EGS participates in system optimization operation utility analysis

All kinds of basic parameters are brought into the day-ahead scheduling model of geothermal RIES with HDR. Scenarios with and without EGS are configured. The cost comparison results of the two scenarios are shown in Table 6.

TABLE 4 EGS system parameters.

m_{HDR}^{min}	m_{HDR}^{max}	α	β	η^{geo}	η^{loss}
35 kg s	45 kg s	0.3	0.6	0.45	0.1

TABLE 5 Price coefficient parameters.

ε	β_e	β_g	p_{gas}
0.032 (元/kg)	0.970 kg/kW h	0.23 kg/kW h	0.35 kg/kW h

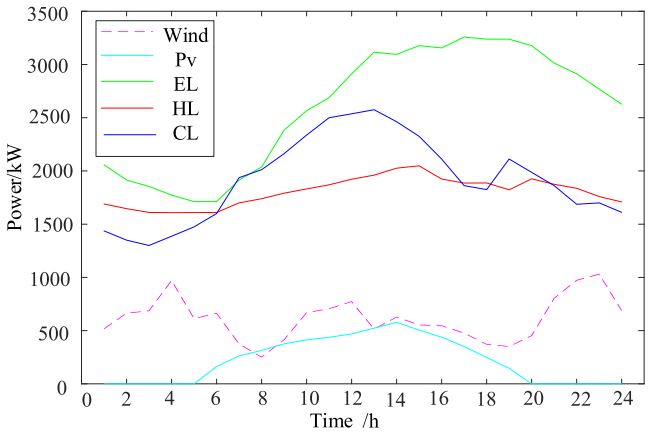

FIGURE 6 Load, photovoltaic and wind power forecast.

It can be seen from Table 6 that when EGS does not participate in system scheduling, the scheduling cost is ¥54,460. When EGS participates in scheduling, the scheduling cost is ¥47,073. The access of EGS reduces the total power purchase of the system within 24 h by 8305 kW, the consumption of natural gas by 3051.9 m^3, and the total carbon emission by 742.28 kg. It achieves the purpose of reducing system cost and energy saving and emission reduction.

The output of each hub before and after the system is connected to EGS is shown in Figure 7 and 8. The impact of EGS participation in system optimization scheduling is reflected in the following aspects:

In terms of electrical and thermal hubs, EGS changes the power structure inside the hub and relieves the pressure on the power supply and system heating. On the supply side, the CHP and GB units are no longer limited by the maximum output. The CHP power supply has been reduced by 6839 kW; the GB heating power has been reduced by 6949 kW. In addition, the system's demand for purchasing power from the grid is reduced. It effectively reduces the purchase cost of electricity and gas. On the demand side, since the excess heat energy of EGS drives the cooling of AC units, the cooling demand for EC units is reduced. The upper limit of demand for electrical load is slightly reduced, while the upper limit of demand for thermal load is increased. In terms of energy storage, the reduction of energy supply pressure reduces the upper limit of the capacity of the energy storage device. The energy balance of the system has become more stable and flexible.

With respect to cold hubs, the excess thermal power of EGS increases the output ratio of AC units during periods of high electricity prices. The output of the AC unit is more stable, and the number of starts and stops is less.

5.2 | IGDT scheduling strategy analysis considering landscape uncertainty

To solve the problem of landscape uncertainty in the system, three different uncertainty scenarios are set

TABLE 6 Cost comparison.

System	Electricity (¥)	Gas (¥)	Carbon emission (¥)	HDR (¥)	Total cost (¥)
Without EGS	16,801	36,148	1511	0	54,460
With EGS	10,402	25,467	1043	10,161	47,073

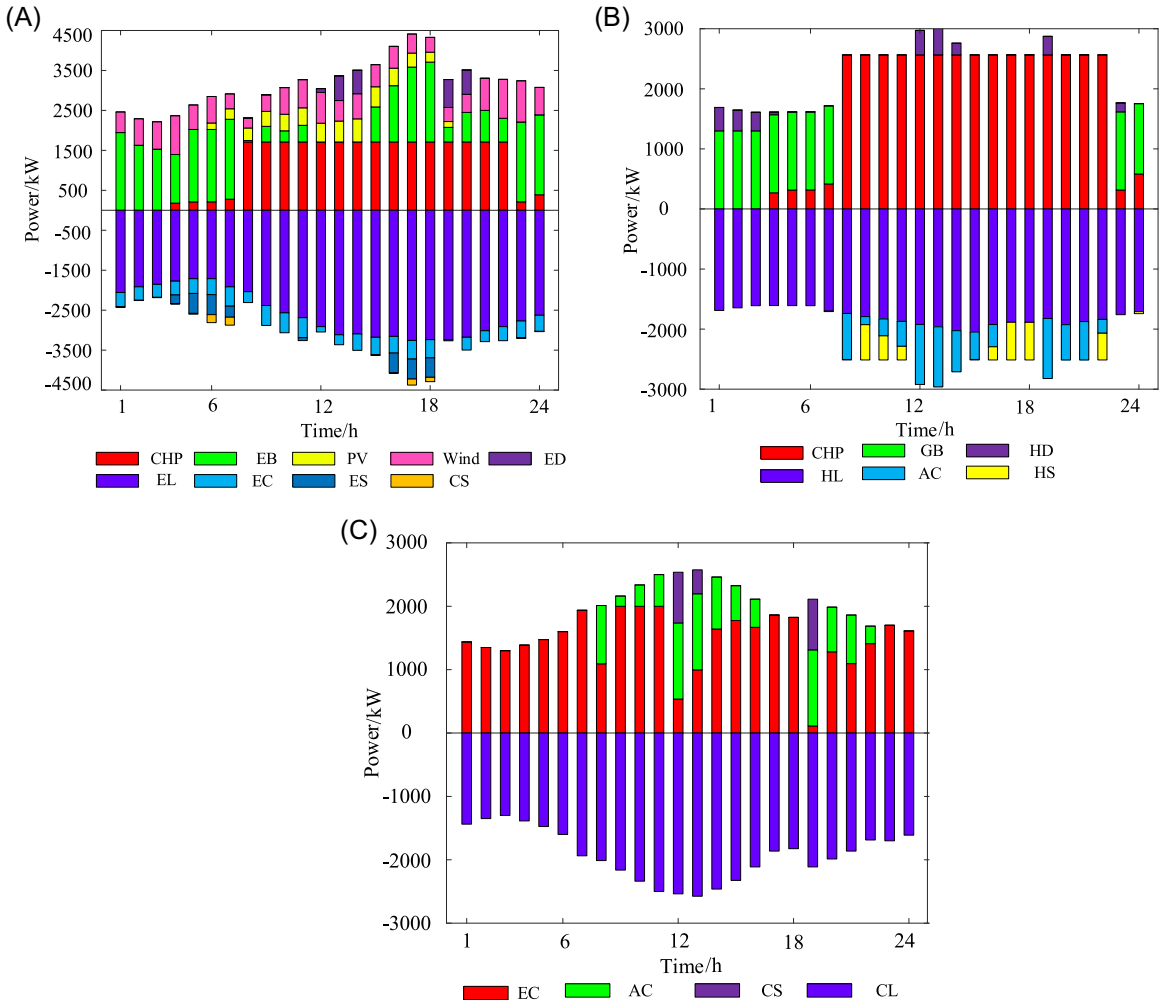

FIGURE 7 Optimal scheduling results of each hub in the traditional system. (A) Power hub scheduling result. (B) Hot hub scheduling result. (C) Cold hub scheduling result.

up. Table 7 illustrates the combination of the three uncertain factors. Where, √ means that the model takes into account the uncertainty. × means that the model does not take into account the uncertainty.

The fluctuation amplitude of uncertainty parameters in IGDT robust model and chance model are assumed to be α_r and α_o. Take the deviation factor set to 0.05 as an example. The pessimistic scheduling cost and optimistic scheduling cost are ¥49,487 and ¥44,774, respectively. Under the two strategies, the wind power uncertainty is $\alpha_r = 19.65\%$ and $\alpha_o = 20.02\%$. The solar power uncertainty is $\alpha_r = 49.25\%$ and $\alpha_o = 51.35\%$. The uncertain output range of wind power and photovoltaic is shown in Figure 9.

At this time, it can be obtained that the output ranges of wind and photovoltaic power in the IGDT robust model are $[0.8135, 1]\widetilde{P_t^w}$ and $[0.5075, 1]\widetilde{P_t^{pv}}$. The output ranges of wind and PV in the IGDT opportunity model are $[1, 1.2002]\widetilde{P_t^w}$ and $[1, 1.5115]\widetilde{P_t^{pv}}$. Compared with other methods of dealing with uncertainty, the biggest advantage of IGDT is to judge the variation range of uncertainty parameters according to the running cost.

5.3 | IGDT decision angle and sensitivity analysis

When the robust deviation factor and opportunity deviation factor vary in the range of 0–0.05, the solution result trajectory of IGDT scheduling model for three uncertain scenarios is shown in Figure 10. The benchmark value f_0 of the scheduling cost in the figure is the benchmark cost obtained by solving the deterministic scheduling model.[26,27]

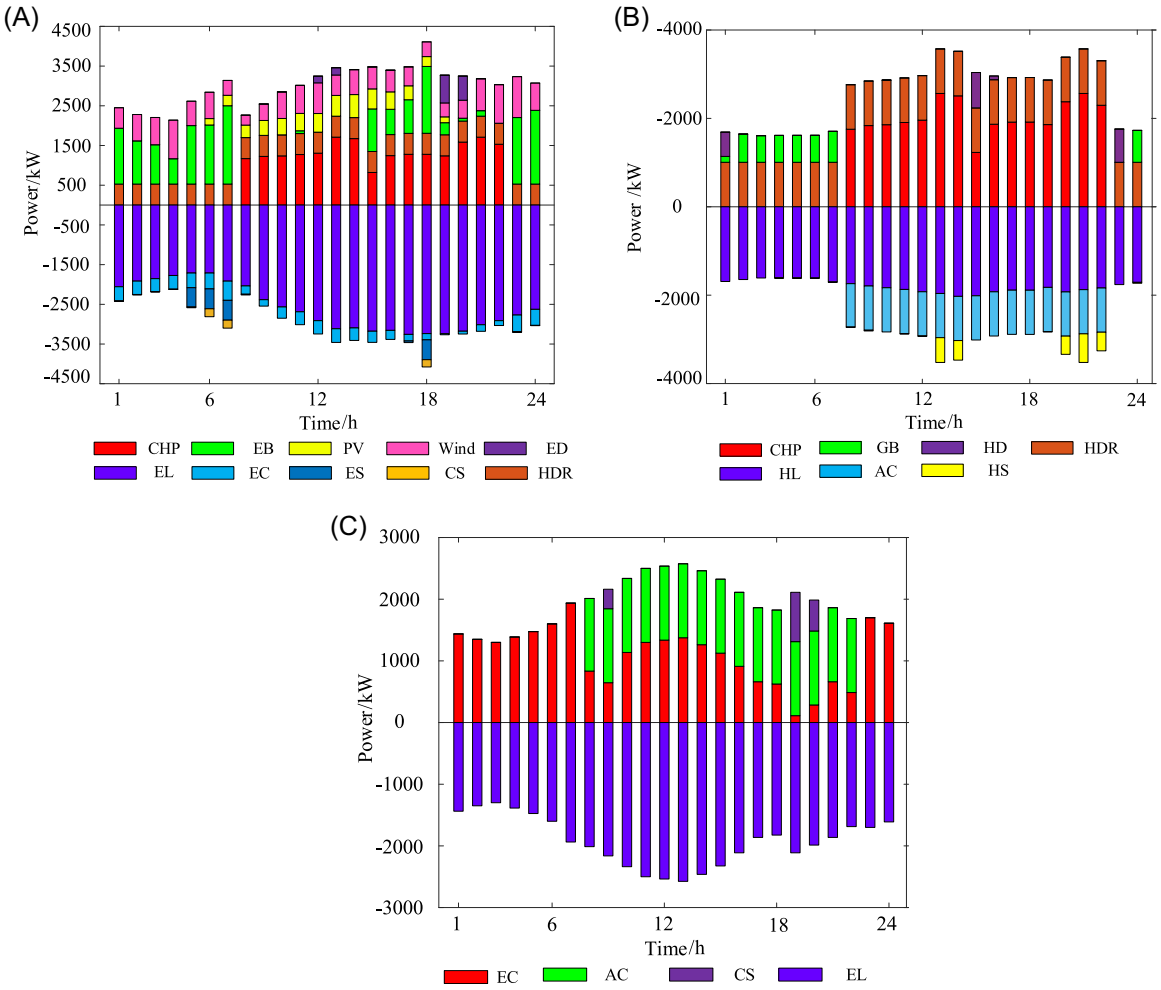

FIGURE 8 Optimization tuning results of each hub in EGS system. (A) Power hub scheduling result. (B) Hot hub scheduling result. (C) Cold hub scheduling result.

TABLE 7 Three uncertainty scenarios.

Scenario	Wind power	Solar power
Scenario 1	√	×
Scenario 2	×	√
Scenario 3	√	√

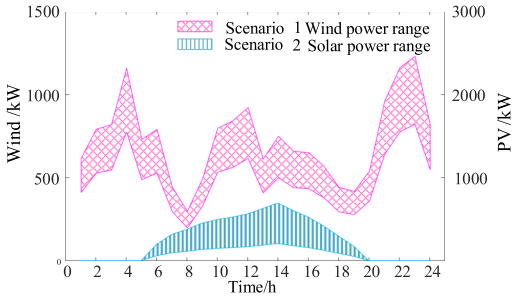

FIGURE 9 Wind power and PV uncertain output range.

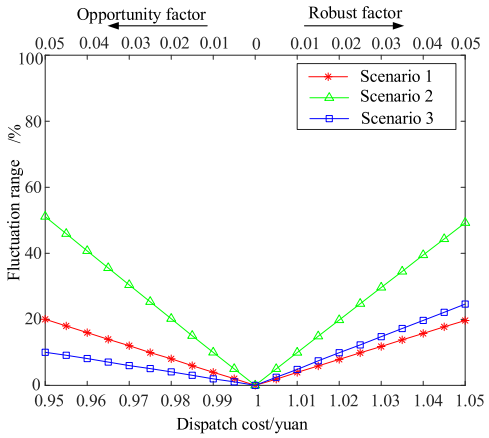

FIGURE 10 IGDT scheduling results of the three scenarios.

From the perspective of system scheduling decision, the fluctuation amplitude α_r and α_o will also increase with the increase of deviation factor. The larger α_r, the greater the gap between uncertainty

TABLE 8 Igdt compared with other random optimization methods.

Method	Uncertainty (%)	Total cost (¥)	Time (s)
Traditional stochastic optimization	25.00	49308	797
Robust optimization	22.64	48653	189
IGDT	19.90	49490	53

changes, and the more pessimistic the decision makers view the fluctuation of uncertainty parameters. The higher the system's robustness, the better its stability. The smaller α_o, the smaller the interval of uncertainty change becomes, and the less optimistic the decision maker is about the income generated by uncertainty parameter fluctuation. The dispatch cost also increases, and system's economy is getting worse.

From the perspective of sensitivity of uncertainty parameters, the larger the value of robust fluctuation ranges α_r under different scenarios, the stronger the system's ability to resist fluctuations. The less sensitive it is to the fluctuation of uncertain parameters, the better the robustness. In different scenarios, the smaller the value of the opportunity fluctuation range α_o, the weaker the system's ability to resist fluctuations. The more sensitive the system is to fluctuations in uncertain parameters, the greater the risk. At the same time, it is more likely to achieve the opportunity target cost.

As can be seen from Table 8, in the process of collaborative optimization of uncertainty and dispatching cost, IGDT has better economic benefits and higher tolerance of uncertainty prediction deviation, and has stronger wind power uncertainty management ability at lower total cost. Compared with traditional stochastic optimization, the optimal scheduling time of IGDT is shorter. Compared with robust optimization, IGDT has certain advantages in scheduling cost.

6 | CONCLUSION AND FUTURE WORK

The HDR achieves cogeneration through EGS with stable output and strong dispatching ability. Integrated energy systems including EGS can effectively relieve the energy supply pressure of the system, which reduces the output ceiling of CHP, GB and other units. At the same time, it can reduce the capacity boundary of the system's energy storage components. When EGS participated in scheduling, the scheduling cost was ¥47,073. The access of EGS reduces the total power purchase of the system within 24 h by 8305 kW, the consumption of natural gas by 3051.9 m^3, and the total carbon emission by 742.28 kg. It achieves the purpose of reducing system cost and energy saving and emission reduction. IGDT strategy quantifies uncertainty from the two directions of risk aversion and risk preference. The relationship between the range of uncertainty parameters and the lowest acceptable cost is described. Thus, it provides an economic and secure decision-making basis for the dispatcher is described.

The conclusion is summarized as follows:

1. As a renewable energy with unique advantages, dry hot rock achieves cogeneration through EGS, with stable output and strong scheduling capacity.
2. The RIES including EGS can effectively alleviate the energy supply pressure of the system, reduce the output ceiling of each unit, and reduce the capacity boundary of the system's energy storage components, so as to achieve the purpose of reducing the system's operating costs and carbon emissions.
3. IGDT strategy quantifies uncertainty from the two directions of risk avoidance and risk preference, and describes the relationship between the variation range of uncertainty parameters and the acceptable minimum cost, so as to provide economic and safe decision-making basis for schedulers.

Because the uncertainties of EGS and load are not taken into account, the IGDT strategy proposed in this paper has some limitations. In addition, the model mainly focuses on day-ahead scheduling, and does not consider day-ahead collaborative optimization. For the follow-up work of EGS, the regenerative power station can be added to further improve the renewable energy consumption capacity and the flexibility of the system. For system optimization, the intra-day rotation optimization scheduling of RIES with EGS will be further studied.

ACKNOWLEDGMENTS

The authors extend their appreciation to King Saud University, Saudi Arabia, for funding this work through Researchers Supporting Project number (RSP2024R164), King Saud University, Riyadh, Saudi Arabia.

ORCID

Mohamed A. Mohamed http://orcid.org/0000-0001-8700-0270
Adrian Ilinca http://orcid.org/0000-0002-8236-2317
Emad Abouel Nasr http://orcid.org/0000-0001-6967-7747

REFERENCES

1. Zahedi R, Yousefi H, Aslani A, Ahmadi R. Numerical analysis of water, energy, and environment nexus in the hybrid thermal and solar multigeneration power plants. *Energy Sci Eng*. 2024;12(5):2037-2051.
2. Zhang ZL, Zhang HJ, Xie B, Zhang XT. Energy scheduling optimization of the integrated energy system with ground source heat pumps. *J Clean Prod*. 2022;365:132758.
3. Wang Q, Xiao Y, Tan H, Mohamed MA. Day-ahead scheduling of rural integrated energy systems based on distributionally robust optimization theory. *Appl Therm Eng*. 2024;246:123001.
4. Olasolo P, Juárez MC, Olasolo J, Morales MP, Valdani D. Economic analysis of enhanced geothermal systems (EGS). A review of software packages for estimating and simulating costs. *Appl Therm Eng*. 2016;104:647-658.
5. Ferrantelli A, Fadejev J, Kurnitski J. A tabulated sizing method for the early stage design of geothermal energy piles including thermal storage. *Energy Build*. 2020;223:110178.
6. Wang Y, Li C, Zhao J, et al. The above-ground strategies to approach the goal of geothermal power generation in China: state of art and future researches. *Renew Sustain Energy Rev*. 2021;138:110557.
7. Tan H, Wang Y, Wang Q, Lin Z, Mohamed MA. Day-ahead dispatch of electricity-hydrogen systems under solid-state transportation mode of hydrogen energy via FV-IGDT approach. *Energy*. 2024;300:131113.
8. Al-Kbodi BH, Rajeh T, Zayed ME, et al. Transient heat transfer simulation, sensitivity analysis, and design optimization of shallow ground heat exchangers with hollow-finned structures for enhanced performance of ground-coupled heat pumps. *Energy Build*. 2024;305:113870.
9. Al-Kbodi BH, Rajeh T, Li Y, Zhao J, Zhao T, Zayed ME. Heat extraction analyses and energy consumption characteristics of novel designs of geothermal borehole heat exchangers with elliptic and oval double U-tube structures. *Appl Therm Eng*. 2023;235:121418.
10. Zayed ME, Shboul B, Yin H, Zhao J, Zayed AAA. Recent advances in geothermal energy reservoirs modeling: challenges and potential of thermo-fluid integrated models for reservoir heat extraction and geothermal energy piles design. *J Energy Storage*. 2023;62:106835.
11. Rajeh T, Al-Kbodi BH, Yang L, Zhao J, Zayed ME. A novel oval-shaped coaxial ground heat exchanger for augmenting the performance of ground-coupled heat pumps: transient heat transfer performance and multi-parameter optimization. *J Build Eng*. 2023;79:107781.
12. Wang L, Li H, Bu X. Thermo-economic investigation of binary flashing cycle for enhanced geothermal system. *Geothermics*. 2021;89(3):101951.
13. Tan H, Li Z, Wang Q, Mohamed MA. A novel forecast scenario-based robust energy management method for integrated rural energy systems with greenhouses. *Appl Energy*. 2023;330:120343.
14. Tu Q, Miao S, Yang Z, Yao F, Lin Y. A collaborative scheduling strategy for power transmission and distribution network considering peakcharge allocation mechanism and key scenarios of wind power. Paper presented at: Proceedings of the CSEE. 2023.
15. Zhang Y, Qian A, Ran H, et al. Economic dispatching of building integrated energy system based on opportunity constrained programming. *Power Grid Technol*. 2019;43(1):108-116.
16. Haris M, Hou MZ, Feng W, Mehmood F, Saleem A. A regenerative enhanced geothermal system for heat and electricity production as well as energy storage. *Renew Energy*. 2022;197:342-358.
17. Fox DB, Sutter D, Beckers KF, et al. Sustainable heat farming: modeling extraction and recovery in discretely fractured geothermal reservoirs. *Geothermics*. 2013;46(apr):42-54.
18. Wu Q, Ren H, Gao W, Weng P, Ren J. Design and operation optimization of organic Rankine cycle coupled trigeneration systems. *Energy*. 2018;142(jan.1):666-677.
19. Wang Y, Du Y, Wang J, Zhao J, Deng S, Yin H. Comparative life cycle assessment of geothermal power generation systems in China. *Resour Conserv Recy*. 2020;155(1):104670.
20. Wang Y, Wang Y, Huang Y, et al. Operation optimization of regional integrated energy system based on the modeling of electricity-thermal-natural gas network. *Appl Energy*. 2019;251:113410.
21. Qiu S, Xu W, Tao Y, Sheng Y, Xu J, Zhang W. A data center energy storage economic analysis model based on information decision theory and demand response. In: Hu C, Cao W, eds. *Conference Proceedings of 2022 2nd International Joint Conference on Energy, Electrical and Power Engineering. CoEEPE 2022*. Springer Nature Singapore; 2022:962-973.
22. Jordehi AR. How to deal with uncertainties in electric power systems? A review. *Renew Sustain Energy Rev*. 2018;96:145-155.
23. Soroudi A, Rabiee A, Keane A. Information gap decision theory approach to deal with wind power uncertainty in unit commitment. *Electric Power Syst Res*. 2017;145:137-148.
24. Amirhossein D, Mohammad J, Behnam M. Short-term scheduling strategy for wind-based energy hub: a hybrid stochastic/IGDT approach. *IEEE Trans Sustain Energy*. 2019;10(1):438-448.
25. Zhong C, Xu T, Yuan Y, Feng B, Yu H. The feasibility of clean power generation from a novel dual-vertical-well enhanced geothermal system (EGS): a case study in the Gonghe Basin, China. *J Clean Prod*. 2022;344:131109.

26. Hamzat AK, Omisanya MI, Sahin AZ, Ropo Oyetunji O, Abolade Olaitan N. Application of nanofluid in solar energy harvesting devices: a comprehensive review. *Energy Convers Manag*. 2022;266:115790.
27. Qi H, Sharaf M, Annuk A, Ilinca A, Mohamed MA. A distributionally robust optimization scheduling model for regional integrated energy systems considering hot dry rock co-generation. *Comput Model Eng Sci*. 2024;140(2): 1387-1404.

How to cite this article: Liu Q, Mohamed MA, Ilinca A, Annuk A, Nasr EA. Optimal scheduling of regional integrated energy systems with hot dry rock enhanced geothermal system based on information gap decision theory. *Energy Sci Eng*. 2024;1-14. doi:10.1002/ese3.1798